Chapter 4: Effect of modelling assumptions on SPNCL performances

This chapter includes a detailed investigation of the effect of different assumptions related to Boussinesq approximation, property variation, bend effect, heat loss, axial fluid and wall conduction on the transient and steady-state characteristics. Effect of assumptions on the performance parameters for different working fluids (water, brines and hybrid nanofluids) and the effect of different heat flux distributions, like the uniform, linear, non-linear, sinusoidal and Gaussian, applied to heater have also been explored.

4.1 Methodology

The considered vertical heating horizontal cooling (VHHC) rectangular SPNCL, having heating, cooling, hot and cold leg sections (dimensions are taken from the experimental setup by Vijayan et al. [97]), is shown in Fig.4.1(a). The heating section is placed at the bottom of the left vertical leg and supplied with constant heat flux, and the cooling section is placed at the top horizontal leg on the Clockwise. A tube-in-tube type heat exchanger is provided for heat removal at the cooling section. The whole loop is properly insulated with the ceramic mat, except for the cooler, to reduce heat loss. In the present analysis, the different primary fluids (Water, EG brine (EG/Water:60/40), PG brine (PG/Water:60/40), Al_2O_3+Cu +Water, Al_2O_3+Cu+EG brine, Al_2O_3+Cu +PG brine) and water are used as secondary (coolant) fluid in the loop.

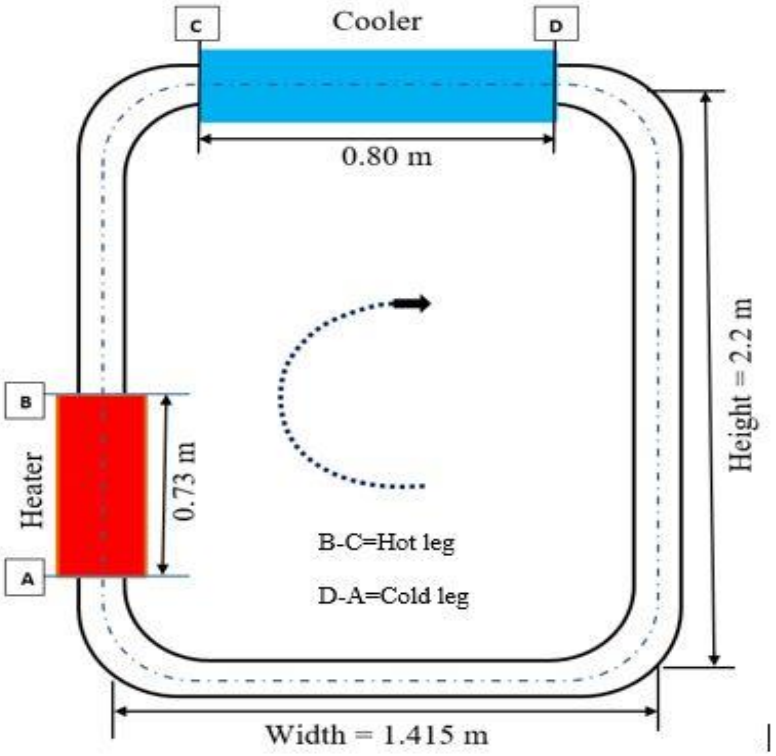
C
Cooler
D
0.80 m
Height = 2.2 m
B
Heater
0.73 m
A
B-C=Hot leg
D-A=Cold leg
Width = 1.415 m

(a)

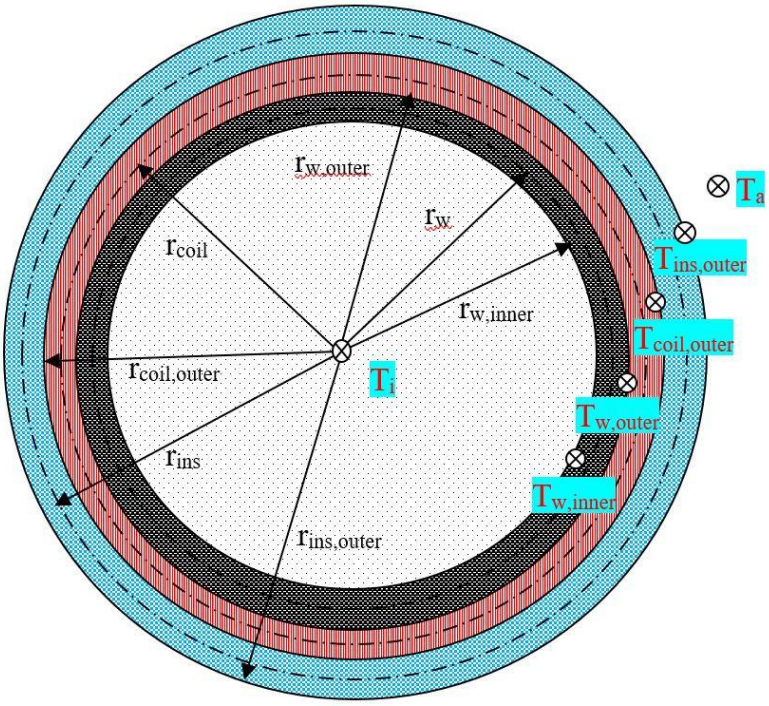
$r_{w,outer}$
r_w
r_{coil}
$r_{w,inner}$
$r_{coil,outer}$
T_i
r_{ins}
$r_{ins,outer}$
T_a
$T_{ins,outer}$
$T_{coil,outer}$
$T_{w,outer}$
$T_{w,inner}$

(b)

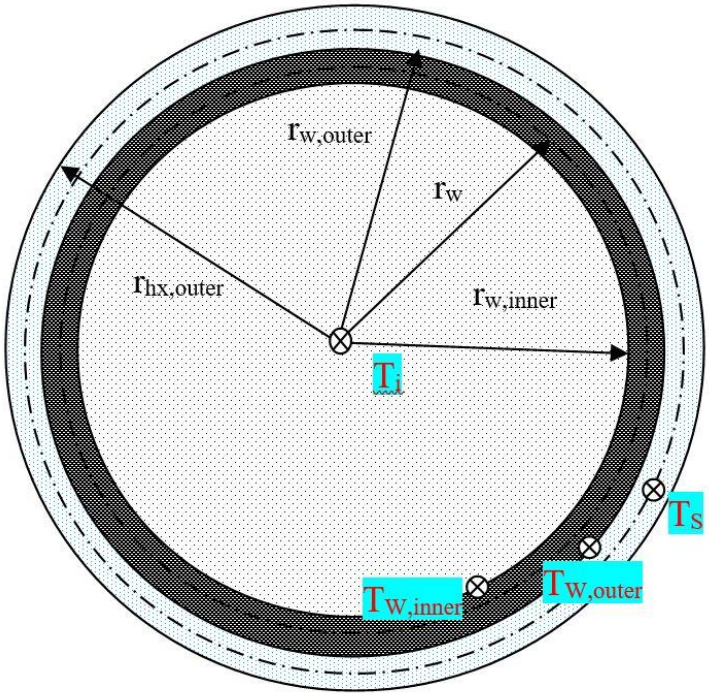

(c)

Fig. 4.1 Schematic illustration of VHHC Single phase natural circulation loop, (b) Cross sectional view of heating section and (c) Cross sectional view of cooler section

4.1.1 Governing Equations:

Governing Equations have been written for 1-D, neglecting the viscous dissipation effect, considering the variation of thermophysical properties with temperature, conduction effect, bend loss, and heat loss.

Mass conservation equation for the primary fluid is given by:

$$\frac{\partial \rho}{\partial t} + \frac{\partial \dot{m}}{A_i \partial s} = 0 \tag{4.1}$$

Momentum conservation equation for the closed loop for the primary fluid is given by:

$$\frac{L_t}{A_i}\frac{\partial \dot{m}}{\partial t} = g\oint \rho \cos(\theta) ds - \left(\frac{fL_t}{d_{W,inner}} + K\right)\frac{\dot{m}^2}{2\rho A_i^2} \tag{4.2}$$

Where θ is the change in the flow direction. For right vertical leg $\theta = 0^o$, top horizontal leg $\theta = 90^o$, left vertical leg $\theta = 180^o$ and bottom horizontal leg $\theta = 270^o$. *K* is the total minor

pressure loss coefficient (3.6) due to four bends (0.9 for each bend). The experimental based empirical value of *K* for 90˚ bend is adopted from Streeter and Wylie [107].

Energy conservation equation for primary (working) fluid in the loop:

$$\frac{\partial(\rho c_p T)_i}{\partial t} + \frac{\partial(\dot{m} c_p T)_i}{A_i \partial s} - \frac{\partial^2 (k_f T)_i}{\partial s^2} = -\frac{U_i \xi_i (T_i - T_W)}{A_i} \tag{4.3}$$

Energy conservation equation for secondary (coolant) fluid in the cooler section:

$$\frac{\partial(\rho c_p T)_S}{\partial t} + \frac{\partial(\dot{m} c_p T)_S}{A_S \partial s} - \frac{\partial^2 (kT)_S}{\partial s^2} = \frac{U_S \xi_S (T_W - T_S)}{A_S} \tag{4.4}$$

Energy conservation equation for heating coil:

$$\frac{\partial(\rho c_p T)_{coil}}{\partial t} - \frac{\partial^2 (kT)_{coil}}{\partial s^2} = -\frac{(T_{coil} - T_W)}{R_{total} V_{coil}} + \frac{Q}{V_{coil}} - \frac{U_o \xi_o (T_{coil} - T_a)}{A_{coil}} \tag{4.5}$$

Energy conservation equation for tube wall for different sections:

$$\frac{\partial(\rho c_p T)_W}{\partial t} - \frac{\partial^2 (kT)_W}{\partial s^2} = -\frac{U_i \xi_i (T_W - T)}{A_W} - \frac{(T_W - T_{coil})}{R_{total} V_W} \qquad \text{Heating section} \tag{4.6}$$

$$\frac{\partial(\rho c_p T)_W}{\partial t} - \frac{\partial^2 (kT)_W}{\partial s^2} = -\frac{U_i \xi_i (T_W - T)}{A_W} - \frac{U_o \xi_o (T_W - T_a)}{A_W} \qquad \text{Hot and cold leg} \tag{4.7}$$

$$\frac{\partial(\rho c_p T)_W}{\partial t} - \frac{\partial^2 (kT)_W}{\partial s^2} = -\frac{U_i \xi_i (T_W - T)}{A_W} - \frac{U_S \xi_S (T_W - T_S)}{A_W} \qquad \text{Heat exchanger} \tag{4.8}$$

The cross-section view of a realistic heater and heat exchanger section is given in Fig.4.1(b) and Fig.4.1(c). This shows the different parts and their arrangement, helps to calculate the overall all heat transfer coefficients (U_i, U_o and U_S) and total conduction resistance (R_{total}) used in the above equations (3-8) using thermal resistance circuit for heating, heat exchanger, hot and cold leg section.

The thermal resistance circuit can be calculated as follows:

For heating section:

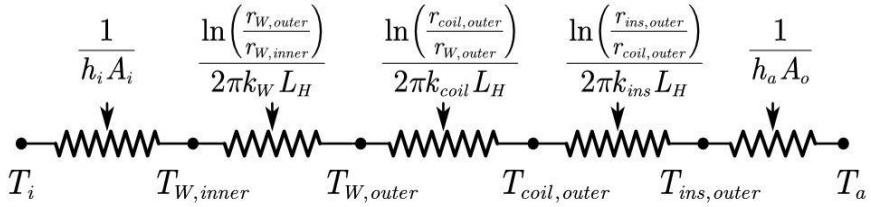

For heat exchanger section:

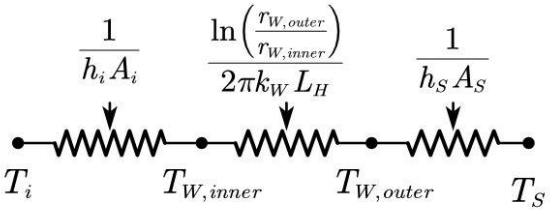

For hot leg and cold leg section:

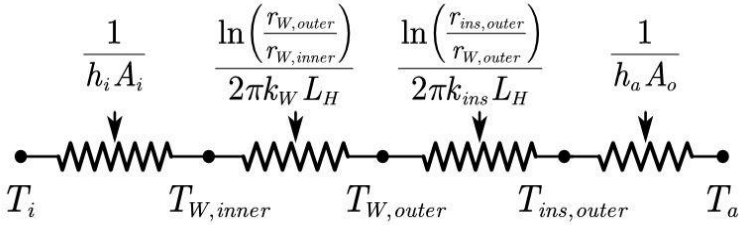

$$\frac{1}{U_i}=\frac{1}{h_i}+\frac{r_{W,inner}\ln\left(\frac{r_W}{r_{W,inner}}\right)}{k_W};\ \frac{1}{U_S}=\frac{r_{W,outer}\ln\left(\frac{r_{W,outer}}{r_W}\right)}{k_W}+\frac{1}{h_S};\ R_{total}=\frac{\ln\left(\frac{r_{W,outer}}{r_W}\right)}{2\pi k_W L_H}+\frac{\ln\left(\frac{r_{coil}}{r_{W,outer}}\right)}{2\pi k_{coil} L_H} \quad (4.9)$$

For heating section:
$$\frac{1}{U_o}=\frac{r_{ins,outer}\ln\left(\frac{r_{coil,outer}}{r_{coil}}\right)}{k_{coil}}+\frac{r_{ins,outer}\ln\left(\frac{r_{ins,outer}}{r_{coil,outer}}\right)}{k_{ins}}+\frac{1}{h_a} \quad (4.10)$$

For Hot and Cold leg section:
$$\frac{1}{U_o}=\frac{r_{ins,outer}\ln\left(\frac{r_{W,outer}}{r_W}\right)}{k_W}+\frac{r_{ins,outer}\ln\left(\frac{r_{ins,outer}}{r_{W,outer}}\right)}{k_{ins}}+\frac{1}{h_a} \quad (4.11)$$

Here, U_i, U_o and U_S is the overall heat transfer coefficient in the primary (working) fluid side, ambient (air) side and secondary (coolant) fluid side, respectively; r_W, r_{coil} and r_{ins} is the mean radius of the internal tube, heating coil and insulation; ξ_i and ξ_S is the inner and outer perimeter of the tube; ξ_o is the perimeter of the insulated tube; h_i and h_s is the heat

convective transfer coefficient associated with the primary fluid and with the secondary fluid, respectively; h_a is the convective heat transfer coefficient associated with the ambient air.

For Boussinesq approximation, density variation is a linear function of temperature in the body force term and is given by $\rho = \rho_0\left[1-\beta\left(T-T_0\right)\right]$. The sink temperature or ambient temperature is considered as reference temperature (a most common choice).

4.1.2 Properties of working fluids

The temperature dependent thermophysical for the base fluids (Water and EG/PG brine) are taken from the EES library.

The thermophysical properties of the binary hybrid nanofluid are calculated by using given following models;

Density:

$$\rho_{hnf} = \phi_1\rho_1 + \phi_2\rho_2 + (1-\phi_1-\phi_2)\rho_{bf} \tag{4.12}$$

Specific heat capacity:

$$(\rho C_p)_{hnf} = \phi_1(\rho C_p)_1 + \phi_2(\rho C_p)_2 + (1-\phi_1-\phi_2)(\rho C_p)_{bf} \tag{4.13}$$

Thermal expansion coefficient:

$$(\rho\beta)_{hnf} = \phi_1(\rho\beta)_1 + \phi_2(\rho\beta)_2 + (1-\phi_1-\phi_2)(\rho\beta)_{bf} \tag{4.14}$$

The effective thermal conductivity is estimated by Maxwell–Garnett model [114]:

$$\frac{k_{hnf}}{k_{bf}} = \frac{\frac{\phi_1k_1+\phi_2k_2}{\phi} + 2k_{bf} + 2(\phi_1k_1+\phi_2k_2) - 2(\phi_1+\phi_2)k_{bf}}{\frac{\phi_1k_1+\phi_2k_2}{\phi} + 2k_{bf} - (\phi_1k_1+\phi_2k_2) + (\phi_1+\phi_2)k_{bf}} \tag{4.15}$$

The effective dynamic viscosity is evaluated by Batchelor equation [115],

$$\mu_{hnf} = \mu_{bf}\left(1+2.5\phi+6.2\phi^2\right) \tag{4.16}$$

where, ϕ_1 =Volume fraction of Al_2O_3, ϕ_2 =Volume fraction of Cu and $\phi = \phi_1 + \phi_2$

Thermo-physical properties of the nanoparticles are shown in Table 4.1.

Table 4.1 Thermophysical properties of nanoparticles [99].

Thermophysical property	Cu (Spherical)	Al_2O_3 (Spherical)
$\rho(kg/m^3)$	8933	3970
$C_p(J/kgK)$	385	765
$k(W/mK)$	400	40
$\beta(K^{-1})$	0.000051	0.000024

4.1.3 Nusselt number and friction factor correlation

Primary fluid:

During the transient phase, the flow regime may change from laminar to transition and finally to turbulent, depending on the geometry of the loop and the heat input. Therefore, a proper estimation of the friction factor and the convective heat transfer coefficient is necessary. The transition occurs at an early stage at the lower Reynolds number for SPNCL [75,21,116]. Hence, the adopted friction factor, along with Reynolds number criteria suitable for numerical simulation to avoid numerical instability, are given by [75]:

$$f_{laminar} = 64/\mathrm{Re} \qquad \mathrm{Re} \le 898 \qquad (4.17)$$

$$f_{transition} = 1.2063/\mathrm{Re}^{0.416} \qquad 898 \le \mathrm{Re} \le 3196 \qquad (4.18)$$

$$f_{turbulent} = 0.316/\mathrm{Re}^{0.25} \qquad \mathrm{Re} \ge 3196 \qquad (4.19)$$

Similarly, for accurate calculation of heat transfer coefficient, we require a Nusselt number correlation proposed for SPNCL. There are Nusselt number correlations available

for SPNCmLs[56,79], which are valid for Fully developed laminar flow at a lower Reynolds number. The present analysis studied at a higher Reynolds number and also the flow regime is in developing flow; hence the available Nusselt correlations are not suitable for the present analysis. Therefore, the Nusselt correlation for straight pipe has been adopted in both laminar and transition/turbulent regimes. Based on the available correlations, there is inconsistency in the Nusselt number correlation from Re = 2300 to 3000, therefore we have extrapolated the Nusselt values in the given range to avoid numerical instability; the interaction point is of laminar and Transition/turbulent Nusselt correlation is considered as a transition point, the transition occurs at Reynolds number of 2500. Correlations are as follows.

Laminar flow regime for base fluids (Water, EG and PG brine)[107]:

$$Nu = 1.86\,\mathrm{Re}^{(1/3)}\,\mathrm{Pr}^{(1/3)}(d/L_C)^{(1/3)} \quad \text{Developing flow for Gz > 10} \tag{4.20}$$

$$Nu = \frac{hd}{k_f} = 3.66 \quad \text{Fully developed flow (isothermal) for } \mathrm{Gz} \le 10 \tag{4.21}$$

where, $Gz = (\pi d / 4L_C)\,\mathrm{Re}\,\mathrm{Pr}$, Re < 2300

Present case applied Re range Re < 2500

Transition/turbulent flow regime for base fluids by Gnielinski [108]:

$$Nu = 0.012(\mathrm{Re}^{0.87} - 280)\,\mathrm{Pr}^{0.4} \tag{4.22}$$

Applicable for, 1.5 < Pr< 500, 3000 ≤ Re ≤ 10^6

Present case applied Re range 2500 ≤ Re ≤ 10^6

Laminar flow regimes for hybrid nanofluids in the developing region is given by [109],

$$Nu_{hnf} = 2.03 Re_{hnf}^{\ 0.293}\,\mathrm{Pr}_{hnf}^{\ 0.6}\,\phi^{0.06}(d/L_c)^{0.37} \tag{4.23}$$

Applicable for, Re < 2500 and 0 ≤ϕ ≤ 6%

Present case applied Re range Re < 2500

Transition/turbulent flow regime for hybrid nanofluids is given by [110],

$$Nu_{hnf} = 0.065(Re_{hnf}^{0.65} - 60.22)(1 + 0.0169\phi^{0.15})\,\mathrm{Pr}_{hnf}^{0.542} \quad (4.24)$$

Applicable for, 3000 < Re_{hnf} < 16,000 and 0< ϕ < 10%

Present case applied Re range 2500 ≤ Re ≤ 16,000

where, $\mathrm{Re}_{hnf} = \dfrac{\dot{m}_{hnf}\, d}{\mu_{hnf} A}$, $\mathrm{Pr}_{hnf} = \dfrac{\mu_{hnf} c_{phnf}}{k_{hnf}}$

Secondary Fluid:

Convective heat transfer coefficient (h_s) for secondary fluid, water, in the cooler, is estimated from the following Nusselt number correlation for fully developed turbulent flow [107]:

$$Nu = 0.023\,\mathrm{Re}^{0.8}\,\mathrm{Pr}^{0.4}$$

Ambient (air) Side:

Heat transfer coefficient (h_a) for air side is obtained by the following Nusselt number correlation in Churchill and Chu [117]:

$$Nu_a = \frac{h_a L}{k_a} = \{0.825 + \frac{0.387 Ra_L^{1/6}}{[1 + (0.492\,\mathrm{Pr}_a)^{9/16}]^{8/27}}\} \quad (4.25)$$

4.1.4 Numerical scheme and performance parameters

In order to solve the coupled equations (1-8), for transient and steady-state conditions, a finite difference-based numerical tool has been developed using Engineering Equation Solver (EES) [111]. The transient terms in the momentum and energy conservation equation are discretized with the first-order implicit scheme. The convective terms in the energy are discretized with the first-order upwind scheme term and the second-order central difference is used for the diffusion term. In the present numerical analysis, the temperature-

dependent thermo-physical properties of considered base fluids are adopted from EES library. Whereas all the thermo-physical properties of the nanofluids are calculated by mathematical models presented in section 4.1.2. The calculation of the performance parameter has been presented in the Chapter 3 section 3.1.4.

Performance para

4.1.5 Grid and time-independent test

In order to eliminate the spatial and temporal discretization error, the grid and time independence test has been performed, as mentioned in chapter 3 (3.1.5).

4.2 Results and Discussion

In the present study, the effect of various cases of assumption on the steady and transient performance of VHHC SPNCL has been discussed. The effect of different natures of heat fluxes distribution such as uniform, linear (increasing and decreasing), non-linear (increasing and decreasing), sinusoidal and Gaussian at the heating section on the performance parameter (mass flow rate, effectiveness and entropy generation) have been studied. In this analysis, different primary fluids such as Water, EG brine (EG/Water:60/40), PG brine (PG/Water:60/40), Al_2O_3+Cu +Water, Al_2O_3+Cu+EG brine, Al_2O_3+Cu +PG brine been used. For each hybrid nanofluid, equal and total (1%) volume concentration of nanoparticles has been selected.

Table 4.2 Considered geometric and operating parameters of VHHC SPNCL.

Input Parameters	Values
Tube material	Borosilicate glass
Heating Coil material	Nichrome
Thickness of heating coil	1 mm

Diameter (internal) of tube	26.9 mm
Thickness of the tube	1 mm
Cooler outer tube diameter (internal)	49.2 mm
Loop Height	2.2m
Loop width	1.415m
Heater length	0.73m
Cooler length	0.80m
Insulation material	Ceramic mat
Coolant mass flow rate	0.3 kg/s
Inlet temperature of the coolant	301K
Pressure inside loop	101.325 kPa
Heater power input	100-1010W
Nanoparticle volume concentration	$\phi = 1\%$

4.2.1 Effect of various assumptions on the performance of VHHC SPNCL

This section deals with the influence of different assumptions and assessment of their validity for predicting the steady-state and transient behaviors of VHHC SPNCL using water as primary fluid. The following six different combinations of assumptions, as in cases (i – vi), are considered:

i. Boussinesq with constant properties + heat loss neglected + bend effect neglected + conduction effect neglected (axial conduction in fluid, wall conduction and heating coil conduction)

ii. Non-Boussinesq with temperature-dependent properties+ heat loss neglected + bend effect neglected + conduction effect neglected

iii. Boussinesq with constant properties + heat loss considered + bend effect neglected + conduction effect neglected

iv. Boussinesq with constant properties + heat loss neglected + bend effect considered + conduction effect neglected

v. Boussinesq with constant properties + heat loss neglected + bend effect neglected + conduction effect considered

vi. Non-Boussinesq with temperature-dependent properties + heat loss considered + bend effect considered + axial conduction considered; this represents the actual practical problem.

Fig.4.2. compares the computed steady-state mass flow rate for different input power and for six different cases (i)- (vi), with the experimental data by Vijayan et al. [97]. The figure shows that case (vi), i.e., Non-Boussinesq with temperature-dependent properties (including heat conduction, bend loss and heat loss), provides a comparatively better agreement with the measured data. The average deviation between the measured and computed values for the steady-state condition is about 9.6%. In particular, case (ii), i.e., Non-Boussinesq with temperature-dependent properties condition over-predicts (maximum 14.2%) and case (i), i.e., Boussinesq approximations with constant properties under-predicts (maximum 30%) the mass flow rate at 1000 W power input compared to case (vi) Non-Boussinesq with temperature-dependent properties (including conduction, bend loss and heat loss). The figure also reveals case (i) Boussinesq with constant properties underpredicts mass flow rate, minimum (6%) at 100 W and it increases with the power input reaches a maximum (30%) at 1000 W compared to case (vi). Including the heat conduction in the Boussinesq increases the mass flow rate, whereas heat loss and bend loss reduce the mass flow rate. But the effect of case (v) conduction effect has very minimum influence on the mass flow rate (2%) followed by case (iii) heat loss (6%) and case (iv)

bend effect (10.6%) compared to the case (i) at 1000 W power input (see. Table 4.3). The conduction effect and heat loss can have a significant influence on the fluids having higher thermal conductivity and are operated at a higher temperature.

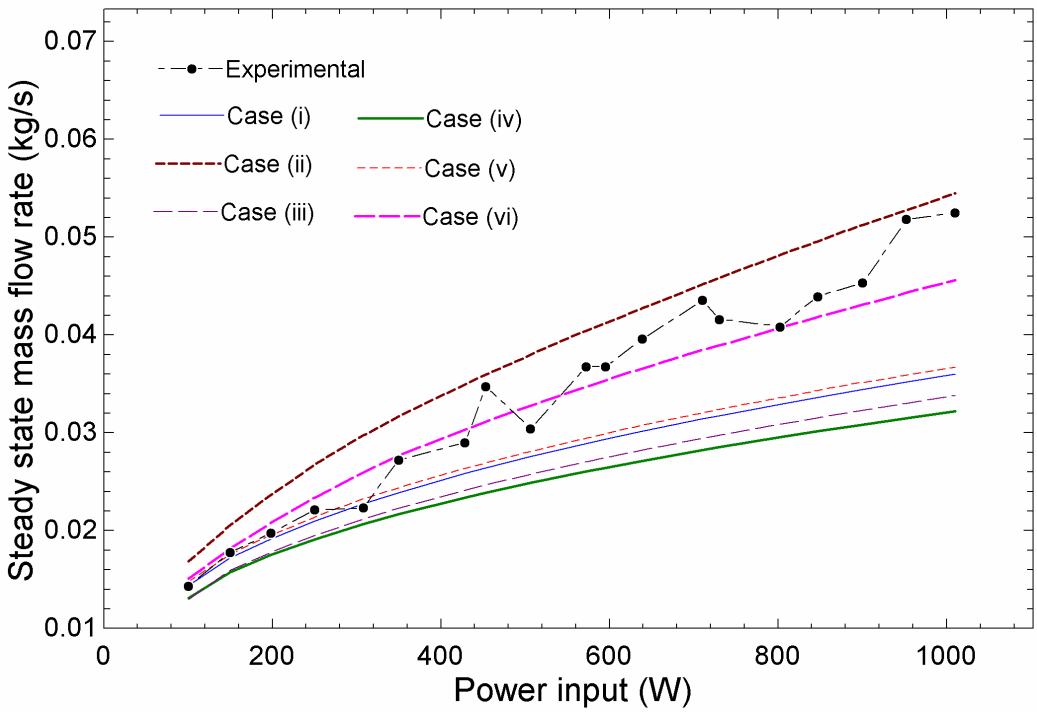

Fig. 4.2 Comparison of steady state mass flow rate obtained numerically for different cases (i-vi) with experimental data [97] using water.

Fig.4.3. shows the effect of different combinations of assumptions, cases (i) to (vi), on the effectiveness of the cooler with power input for water as primary fluid. The figure depicts that the effectiveness of the cooler decreases with the power input. This is attributed to a reduction in the residence time of the hot fluid inside the cooler as a consequence of an enhanced mass flow rate for input power. Since the effectiveness is affected by the heat transfer coefficient, which depends on the Nusselt number correlation. The maximum Reynolds number obtained for each case at 1000 W power input, for case (i) 2020, case(ii) 6420, case (iii) 1905, case (iv) 1815, case (v) 2070 and case (vi) 5203 respectively. Decreasing and increasing trend of effectiveness is observed with power input between 300 W (Re = 2490) and 420 W (Re = 2512) for case (ii) and case (vi), respectively, which is

attributed due to the switching of Nusselt number correlation (at Re=2500). The effectiveness increases for case (iii) heat loss and case (iv) bend effect and decreases for case (v) conduction effect compared to the case (i) Boussinesq approximation with constant properties. An explanation is that the numerator term of the effectiveness equation (4.26) increases in case (iv) and decreases in case (v) due to reduction and increase in mass flow rate, resulting in an increase and decrease in effectiveness, respectively. Whereas, in case (iii), the temperature difference between the cooler inlet and outlet decreases, which decreases the numerator term, and the inlet temperature at the cooler decreases, which decreases the denominator term, as a relative consequence, the effectiveness of the cooler increases. The maximum increase in the effectiveness is observed for case (ii) i,e Non-Boussinesq with temperature-dependent properties (11%) followed by the case (iv) bend loss (8.6%) and case (iii) heat loss (3.5%). Whereas, the maximum reduction in effectiveness is for case (v) conduction effect (5.3%) at 1000 W power input.

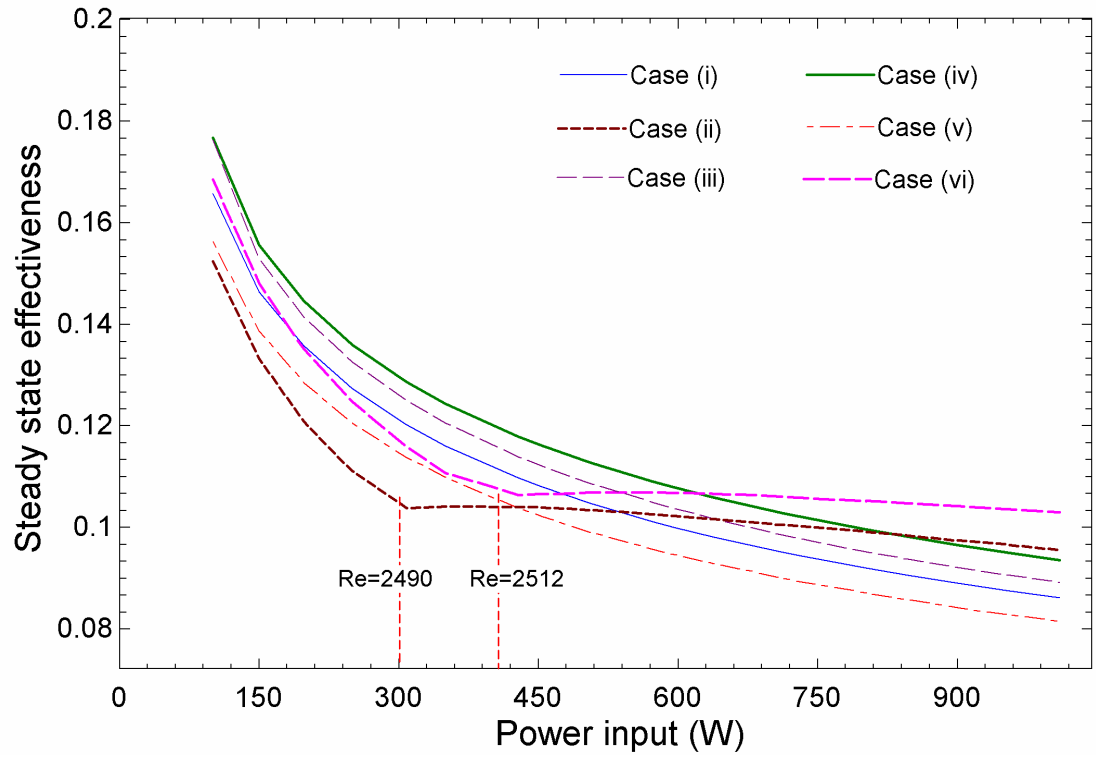

Fig. 4.3 Effect of different cases (i-vi) on steady state effectiveness of cooler with power input.

Fig.4.4. shows the effect of a different combination of assumptions, cases (i) to (vi), on the total entropy generation rate with power input for water. The figure illustrates that the total entropy generation increases with the power input. This is because the cause of entropy generation is the irreversibility linked with the heat transfer and pressure drop. Both heat transfer rate and pressure drop (due to increased mass flow rate) increase with power input and the irreversibility associated with it also increases; hence the total entropy generation rate increases. The total entropy generation is lowest for case (vi) Non-Boussinesq with temperature-dependent properties (including conduction, bend loss and heat loss) shows that the other assumption overpredicts the total entropy generation rate. The conduction effect and bend loss increase the total entropy generation, whereas heat loss decreases the total entropy generation.

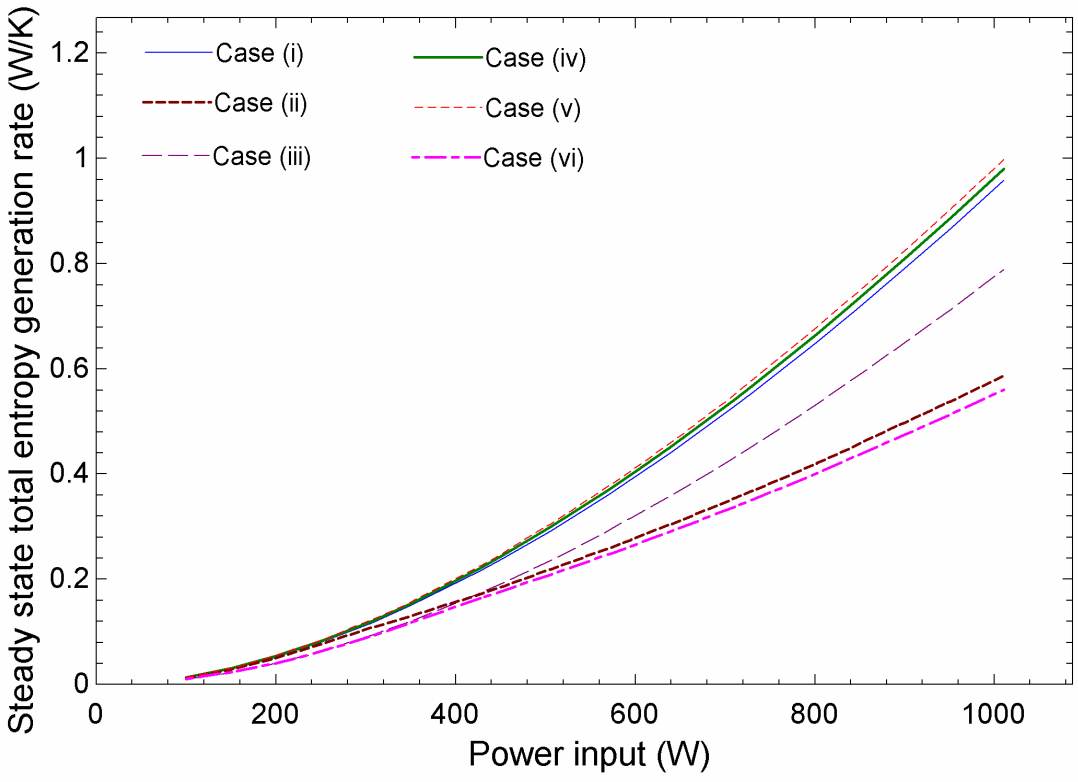

Fig. 4.4 Effect of different cases (i-vi) on steady-state total entropy generation rate with power input.

Fig.4.5 Illustrates the comparison of transient pressure drop for all the combinations of assumptions, cases (i) to (vi), in the present simulation with the experimental result by Vijayan et al. [97] at 530 W using water as working fluid. Pressure drop is calculated over a length of 1065 mm in the bottom horizontal leg. The figure reveals that numerical temporal pressure drops for case (vi) Non-Boussinesq with temperature-dependent properties (including conduction, bend loss and heat loss) compare well matched with the experimental data and have a maximum deviation in the pressure drop of about 12%. Whereas the time deviation to reach the maximum pressure drop is 9%. It can be observed that initially, there is a time lag in the pressure drop between numerical and experimental results for the cases of assumption, which does not have the conduction effect. This is attributed to the incurred delaying in transferring the supplied input power, by way of an electrical heater, to the working fluid in SPNCL via an external heat exchanger. Hence the temperature of the fluid increases instantaneously, and flow is initiated. Consequently, a sudden increase in pressure drop is observed. While considering the conduction effect, the time lag decreases because of the heating coil and wall conduction effect, in which the heat is generated in the heating coil, transferring the heat from the heating coil to the wall by conduction and then the from wall to the primary fluid by convection, which takes some time to diffuse heat due to thermal inertia (wall and heating coil) and thermal resistance from heating coil to the primary fluid. The result reveals that the conduction effect has a significant influence on the transient behavior of the loop.

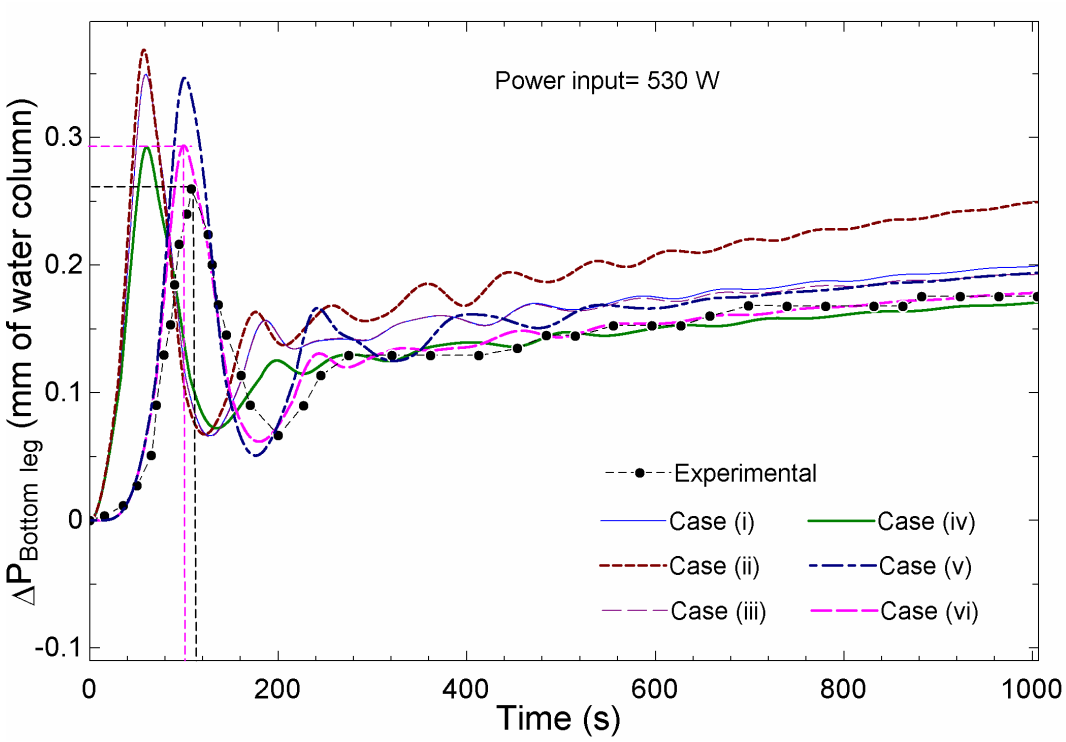

Fig. 4.5 Comparison of transient pressure drop obtained by different cases (i-vi) with experimental data [97] using water.

Fig.4.6. Illustrates the transient variation of mass flow rate for cases (i) to (vi) at an input power of 530 W for water. This figure reveals that case (ii), Non-Boussinesq with temperature-dependent properties has the highest fluctuation of mass flow rate, and therefore takes a longer duration, compare to other cases, to attain the steady-state condition. The case (iv) effect of bend reduces the fluctuations and stabilizes the flow at an early instant of time. In case (v), the conduction effect increases the flow initiation time compared to case (i) Boussinesq approximation with constant properties.

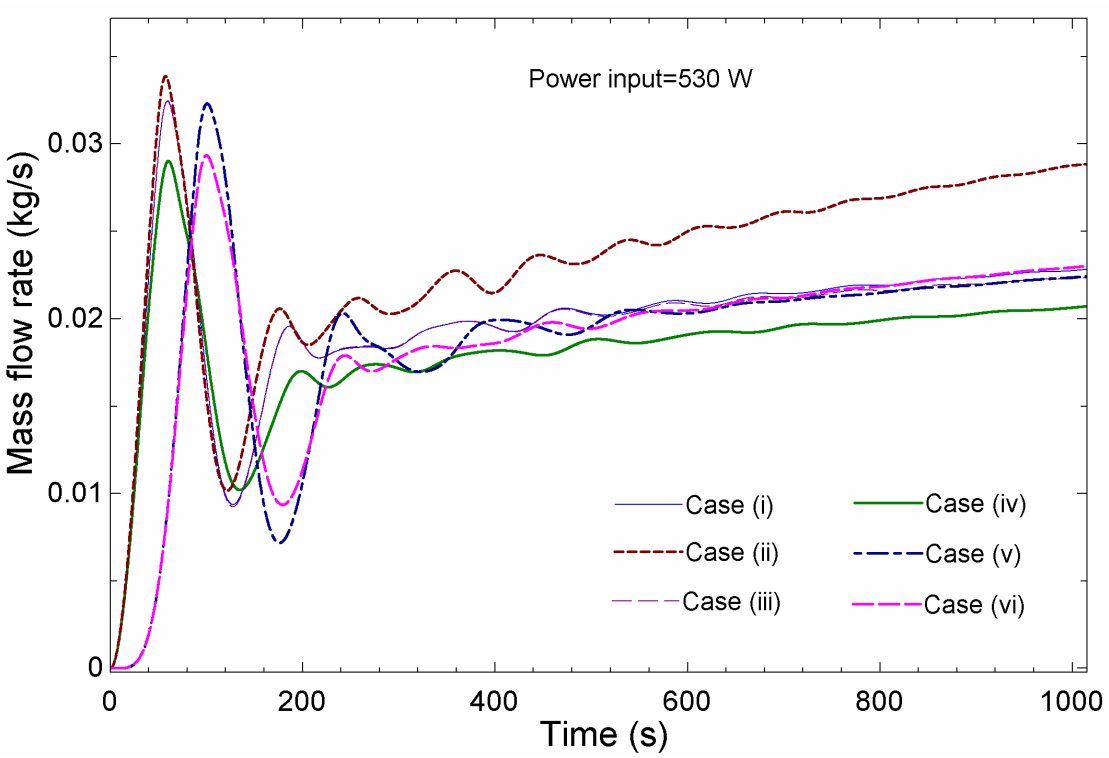

Fig. 4.6 Effect of different cases (i-vi) on the transient mass flow rate

Table 4.3 The effect of different cases (ii-vi) on the performance parameter compared to case(i) at 1000 W power input.

Cases of assumptions	Increment (↑) or Decrement (↓) in Performance parameters compared to case (i)								
	Mass flow rate (%)			Effectiveness (%)			Total entropy generation (%)		
	Water	EG brine	PG brine	Water	EG brine	PG brine	Water	EG brine	PG brine
Case (ii)	47.5 (↑)	73.65 (↑)	120 (↑)	11 (↑)	22.3 (↓)	34.83 (↓)	40.8 (↓)	26.38 (↓)	28.4 (↓)

Case (iii)	6 (↓)	10.85 (↓)	12.6 (↓)	3.5(↑)	12.5(↑)	13.9(↑)	17.6 (↓)	23.75 (↓)	24.7 (↓)
Case (iv	10.6 (↓)	4.83 (↓)	2.42 (↓)	8.6(↑)	3.6(↑)	1.8(↑)	2.3(↑)	0.85(↑)	0.43(↑)
Case (v)	2(↑)	2.45(↑)	2.56(↑)	5.3(↓)	5.6(↓)	5.68(↓)	4.2(↑)	3.75(↑)	3.63(↑)
Case (vi)	30(↑)	40(↑)	78.2(↑)	20(↑)	19.4(↓)	32.70(↓)	38.3(↓)	32.32(↓)	34.73(↓)

4.2.2 Effect of different working fluids on the performance of VHHC SPNCL

In this section, the percentage deviation in the performance parameters for case (i) Boussinesq approximation with constant properties compared to the case (vi) Non-Boussinesq with temperature-dependent properties (including conduction effect, bend effect and heat loss) has been calculated for the different primary fluids (Water, EG brine, PG brine, Al_2O_3+Cu +Water, Al_2O_3+Cu+EG brine, Al_2O_3+Cu +PG brine) for different power input.

Fig.4.7 illustrates the relative deviation (with respect to case (i)) in mass flow rate for different power input and base fluids. The positive deviation infers an increase in mass flow rate. It may be argued that (a) a low thermal conductivity leads to a reduced conduction effect, (b) higher heat loss reduces the (c) a higher bend effect, are non-conducive to the observation; therefore, the increase is attributed to the use of the non-Boussinesq with temperature-dependent properties. The maximum deviation for the mass flow rate is the highest for PG brine/PG brine-based hybrid nanofluid (about 78.2%), followed by EG

brine/ EG brine-based hybrid nanofluid (about 40%), water/water-based hybrid nanofluid (about 30%), as shown in Table 4.3.

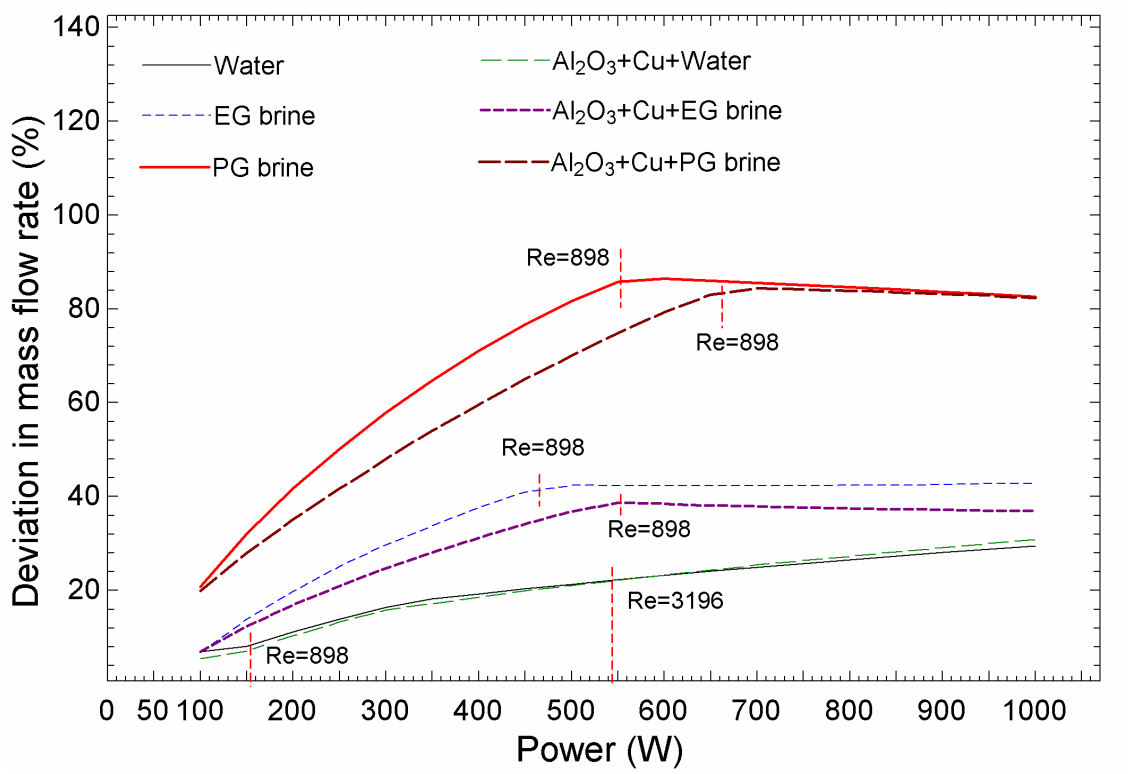

Fig. 4.7 Effect of different base fluids on deviation in mass flow rate with power input

It may be noted that the change of thermo-physical properties for EG/PG brine with temperature is much higher than that of water, as shown in the Fig.4.8(a-d). Thus, the use of Boussinesq approximation with constant properties is not recommended for EG/PG brine and EG/PG brine-based hybrid nanofluids. Such an approximation will lead to a substantial under-prediction of mass flow rate or the equivalent heat transfer for NCL. It can be also observed that between 400-700 W, the deviation in mass flow rate decreases for EG and PG brine and their hybrid nanofluids. The flow regime changes from laminar to transition (achieved at different power input for different fluids) as described in Eq. (4.17-4.19), which decreases the mass flow rate due to increased friction factor. For water and their nanofluids, the transition occurs at a much lower power input than brines (*Re* range for EG and PG brines are 178–2362 and 98–2217, respectively).

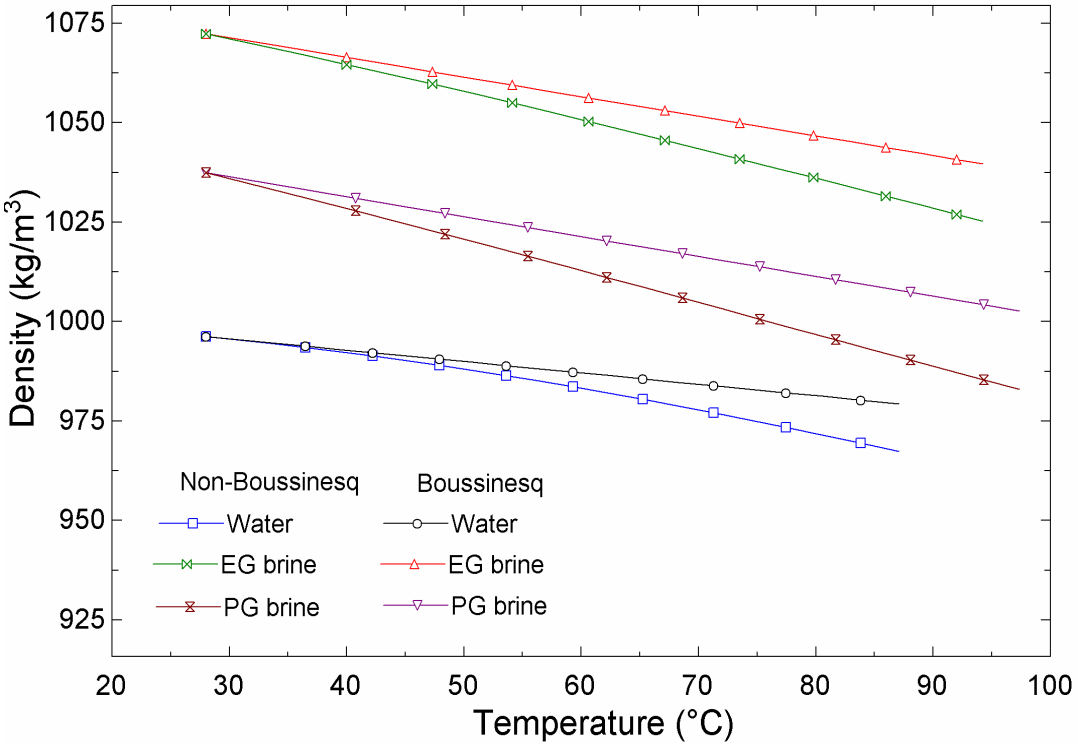

Fig.4.8(a)

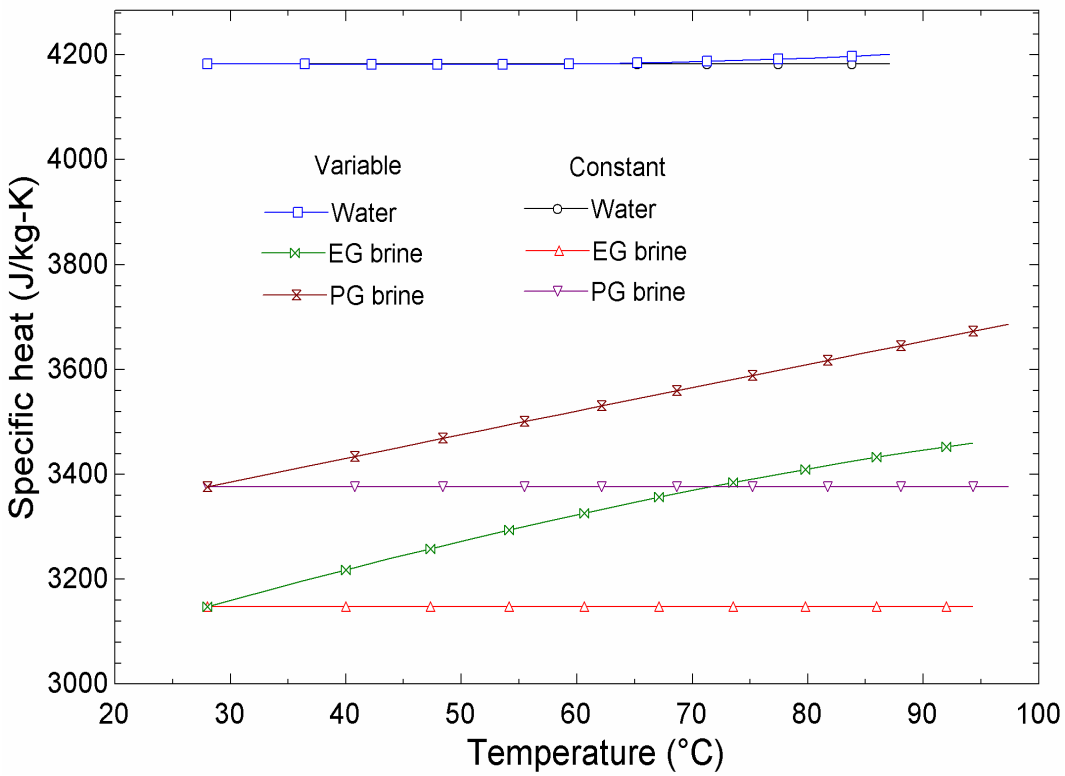

Fig.4.8(b)

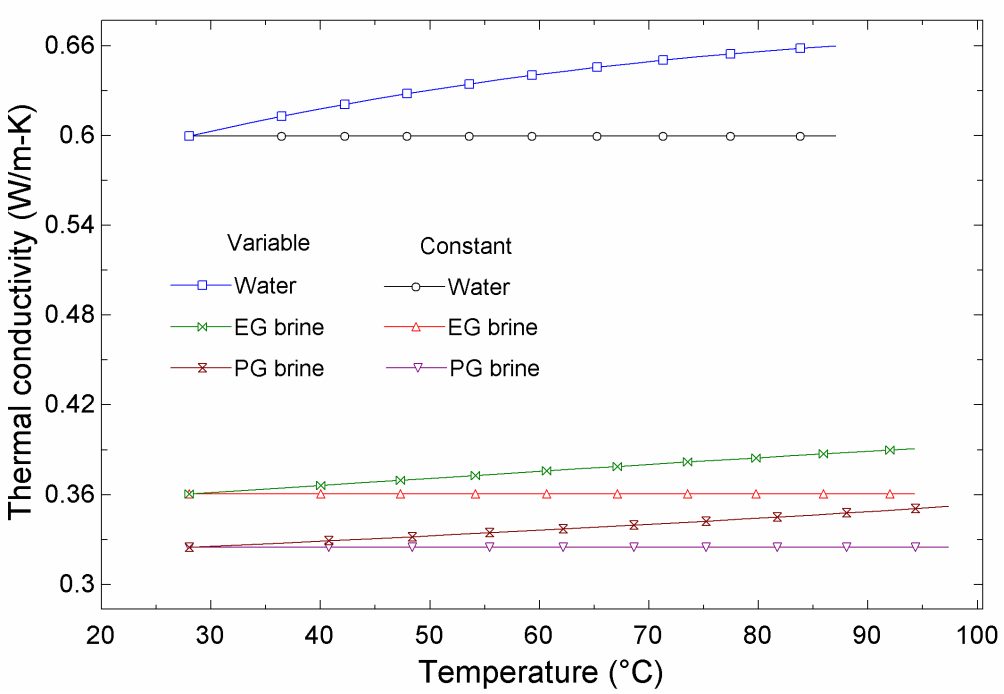

Fig.4.8(c)

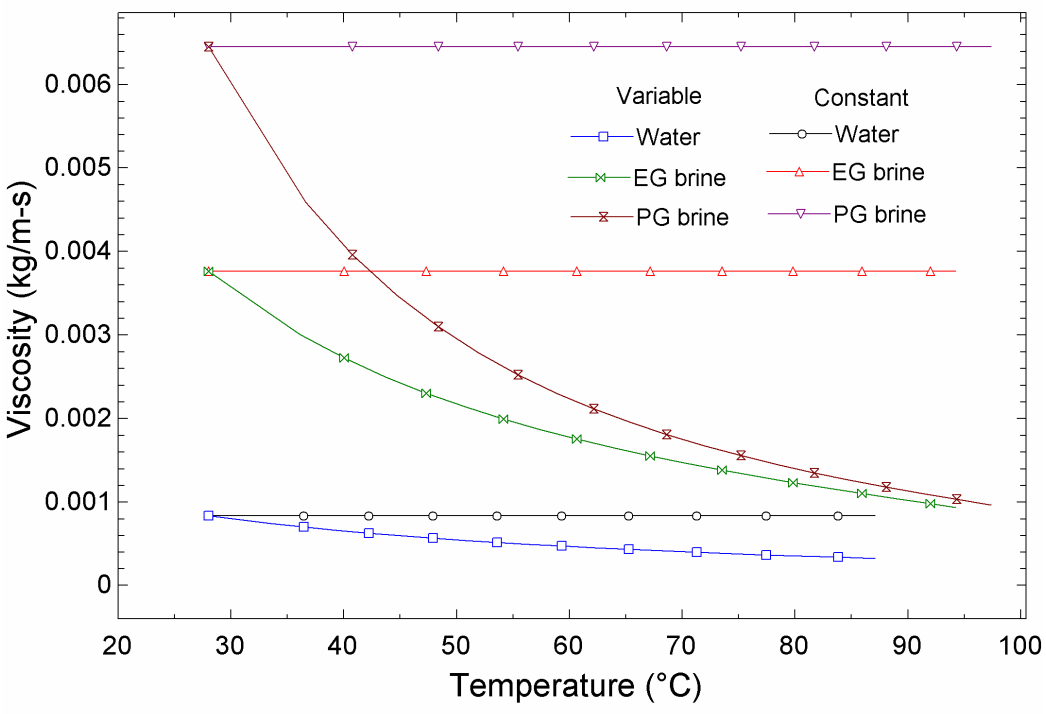

Fig.4.8(d)

Fig. 4.8 Show the constant and variable thermophysical properties variation with temperature, (a) Density, (b) Specific heat, (c) thermal conductivity, and (d) Viscosity of the different base fluids respectively.

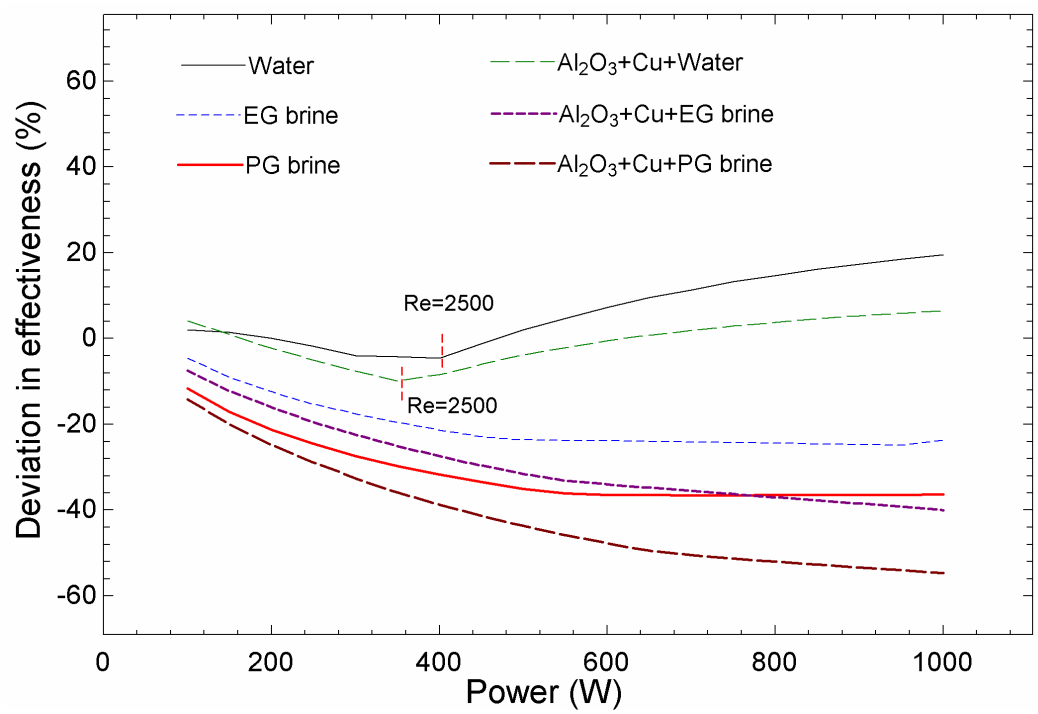

Fig. 4.9 Effect of different working fluids on deviation in effectiveness with power input.

Fig.4.9 illustrates the relative deviation of the calculated effectiveness, between case (vi) and case (i), for different power input and working fluids. The negative values of relative deviation mean that case (i) with Boussinesq approximation with constant properties overpredicts the value of effectiveness with respect to case (vi) with a non-Boussinesq with temperature-dependent properties, including all effects. The figure reveals that (i) the relative deviation is negative for EG/PG brine and EG/PG brine-based hybrid nanofluids and (ii) the negative and then positive (after 400 W) relative deviation is observed for water and water-based hybrid nanofluids. The negative deviation is achieved when increases in the effectiveness due to bend effect and heat loss is lower than the reduction in effectiveness due to Non-Boussinesq with temperature-dependent properties and conduction effect, compared to Boussinesq approximation with constant properties. Similarly, for positive deviation in effectiveness, case (vi) Non-Boussinesq with temperature-dependent properties (including conduction, bend loss and heat loss) has higher effectiveness than the Boussinesq approximation with constant properties. it is

achieved when an increase in the effectiveness due to bend effect, heat loss and Non-Boussinesq with temperature-dependent properties is higher than the decrease in the effectiveness due to the conduction effect compared to Boussinesq approximation with temperature-dependent properties (see Fig.4.3 and Table 4.3). Water and Al_2O_3+Cu+water show decreasing and then increasing trend in the deviation of effectiveness at 350-400 W (corresponding Re=2500), which may be due to the fact the effectiveness strongly influenced by the heat transfer coefficient, and the due to change in the Nusselt correlation at Re=2500, sudden change in effectiveness is observed. which is consistent with Fig.4.3. Whereas, for EG, PG brines and their based hybrid nanofluids yield consistent trend because maximum Reynold number at 1000 W is below 2500.

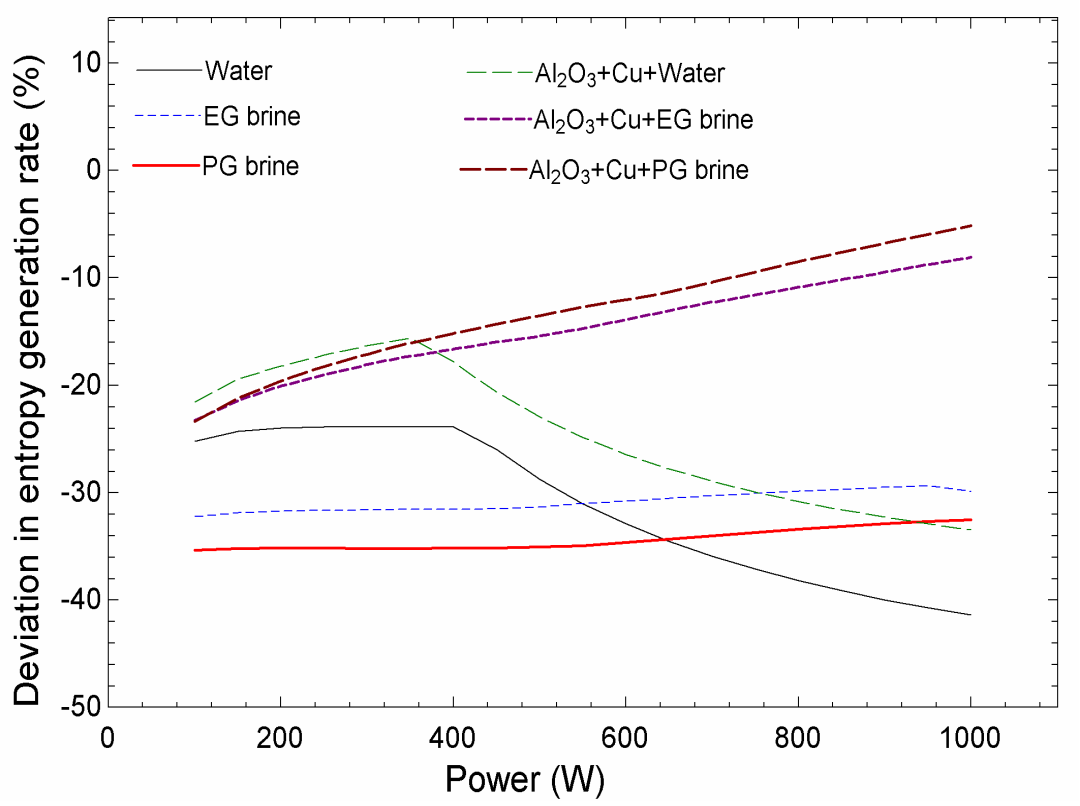

Fig. 4.10 Deviation in entropy generation with power input for different working fluids

Fig.4.10 illustrates the deviation in total entropy generation with power input for different working fluids. The figure shows that the deviation in total entropy generation is negative, or over-prediction with Boussinesq approximation with constant properties, for

all the working fluids. This is because the increases in the entropy generation due to bend effect and conduction effect is lower than the reduction in entropy generation due to Non-Boussinesq with temperature-dependent properties and heat loss compared to Boussinesq approximation with constant properties (Table 4.3). The possible reason is that the entropy generation increases with higher temperature difference (T_{out}-T_{in}), temperature ratio (T_{out}/T_{in}), the heater's wall temperature, and cooler and pressure drop. For case (i) with Boussinesq approximation with constant properties, the highest total entropy generation rate, is attributed to the lowest mass flow rate, resulting higher temperature difference (T_{out}-T_{in}), temperature ratio (T_{out}/T_{in}) ratio, and wall temperature at a given power, in comparison to case (vi) Non-Boussinesq with temperature-dependent properties (including other effects). However, the entropy generation due to the pressure drop of Boussinesq approximation with constant properties is lower due to low mass flow, but its value is insignificant compared to other parameters. The base fluids show a higher deviation in the total entropy generation compared to their based hybrid nanofluid.

Fig.4.11 illustrates the transient mass flow rate for different working fluids at 500 W power input for case (i) Boussinesq approximation with constant properties, blue lines. and for case (vi) non-Boussinesq with temperature-dependent properties (including conduction effect, bend effect and heat loss), black lines. The figure shows that case (i) underpredicts the fluid flow initiation time duration for all the fluids, whereas overpredicts the fluctuation in mass flow rate for all the fluids except for PG brine Al_2O_3+Cu +PG brine compared to case (vi). The maximum deviation in mass flow rate is about 13% (underprediction) for PG brine and 10% (overprediction) for water, whereas the maximum and minimum underprediction in the time deviation is 76% for EG brine and 33% Al_2O_3+Cu +PG brine respectively. The hybrid nanofluids show early development fluid flow and attain stability at the early instant; and has a higher mass flow rate compared to

the base fluid, which is consistent with the finding of Bejjam et al. [55]. This shows that hybrid nanofluid has a significant influence on the transient characteristics of the SPNCL system and can be crucial for eliminating the stability issue.

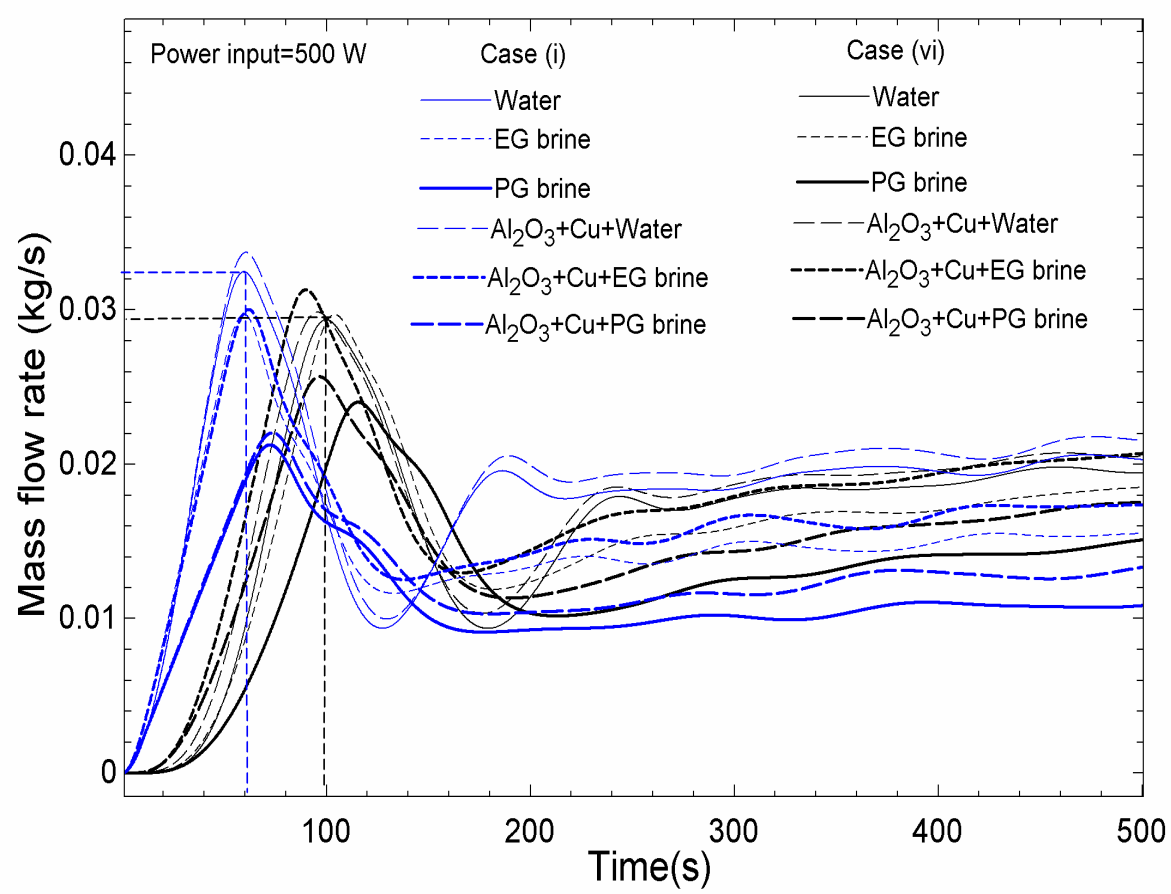

Fig. 4.11 Comparison of transient mass flow rate of case (i) and case (vi) for different working fluids.

4.2.3 Influence of different nature of heat flux distribution on the performance parameters

This section reports the performed simulations for the non-Boussinesq with temperature-dependent properties (including conduction effect, bend effect) and Al_2O_3+Cu +Water hybrid nanofluid. Here, the effect of different nature of heat flux distribution, along the heating length for given total input power, on the steady and transient behavior of

VHHC SPNCL, has been presented. The considered heat flux distributions, as in Fig.4.12, are as follows:

Uniform heat flux (Constant): $q_{mean} = Q/(\pi D L_H)$

Linear increasing heat flux (zero to maximum): $q = q_1 + \frac{(q_2 - q_1)}{L_H} x$

Linear decreasing heat flux (maximum to zero): $q = q_2 - \frac{(q_2 - q_1)x}{L_H}$

Where, q_1=0, q_2=2q_{mean}

Non-linear increasing (zero to maximum): $q = q_{max} x^2$

Non-linear decreasing (maximum to zero): $q = q_{max}(L_H - x)^2$

Sinusoidal: $q = q_{mean} + q_{amp} \sin x$, Where, q_{amp} = q_{mean}

Gaussian-type distribution (maximum at the center and tending to zero at both the ends):

$q = q_{max} \exp(-\frac{(x - \frac{L_H}{2})^2}{2\sigma^2})$, Where, σ=0.1

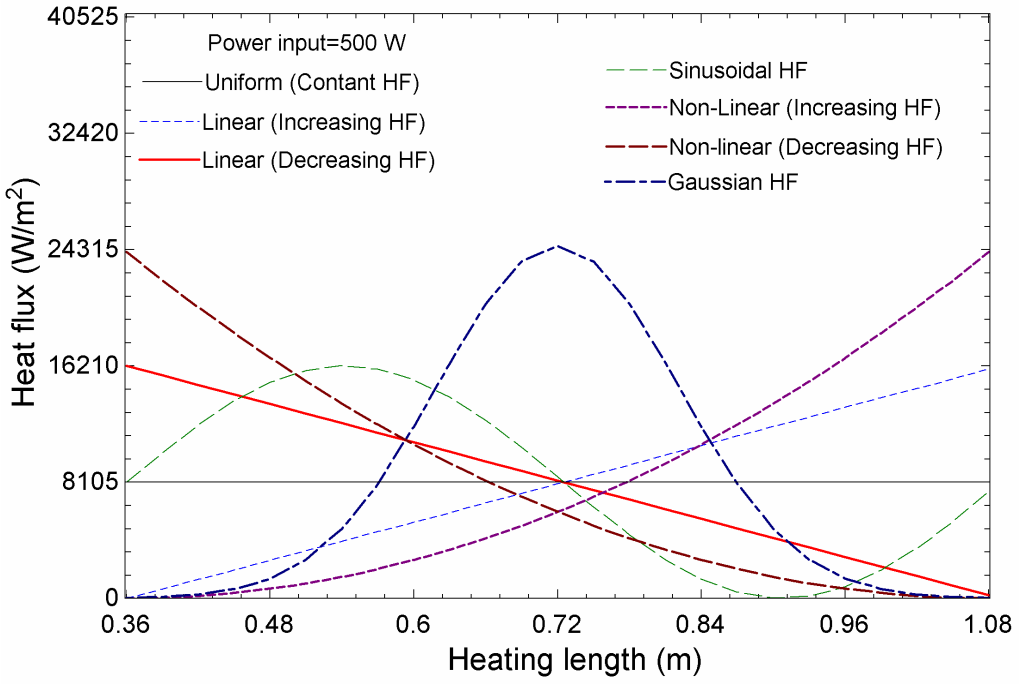

Fig. 4.12 Different heat flux distribution nature along the heating length

Fig.4.13 depicts the transient mass low rate for different nature of heat fluxes applied in the heating section for Al_2O_3+Cu +Water. It demonstrates that the initial fluctuation in the mass flow rate and the time required to attain a steady-state is the highest for non-linearly decreasing heat flux and the lowest for the non-linearly increasing heat flux. The possible reason may be in case of non-linearly decreasing heat flux; the higher heat flux is provided at the entry side of the heating section, so the fluid getting more heat from the beginning of the heater, which increases the effective height of between the heater and cooler, which increases the buoyancy force. Similarly, for non-linearly increasing heat flux, the effective height between the heater and cooler decreases, which reduces the buoyancy force.

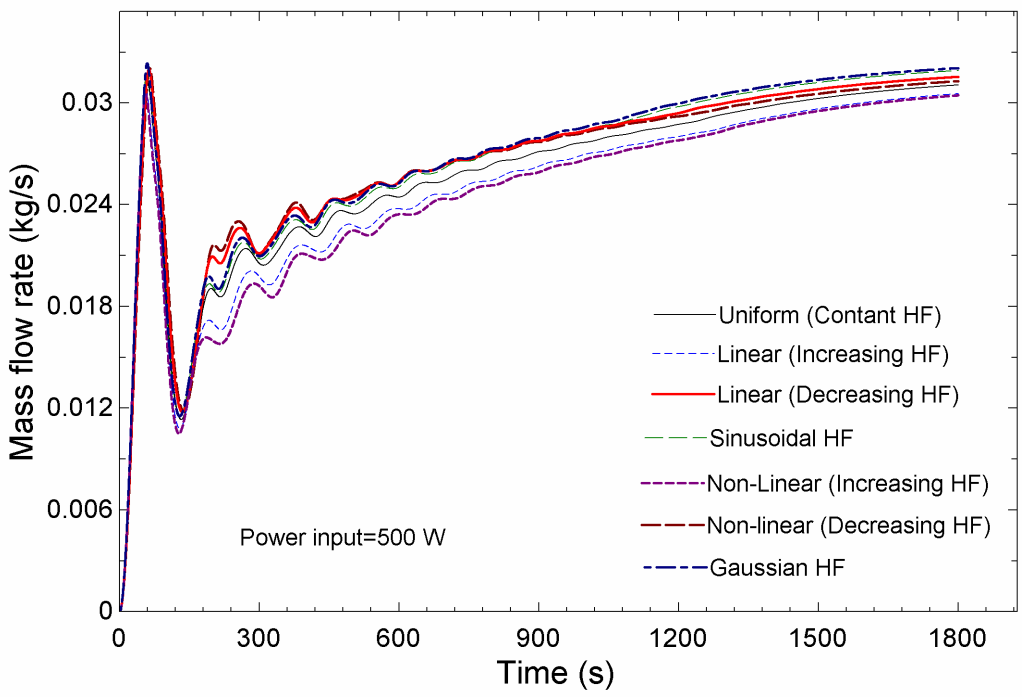

Fig. 4.13 Effect of different heat flux distribution nature on transient mass flow rate for Al_2O_3+Cu +Water

Fig.4.14 illustrates the steady-state mass flow rate for different nature of heat flux distribution for given power input and Al_2O_3+Cu +Water hybrid nanofluids. It can be observed that the mass flow rate increases with heater power input due to the development

of a higher temperature difference between hot leg and cold leg, which increases the bouncy force. At a given power input, the mass flow rate increases for Gaussian, Sinusoidal, linear decreasing and non-linear decreasing heat flux distribution compared to uniform heat flux distribution. Whereas, the mass flow rate decreases for linearly and non-linear increasing heat flux distributions. This is due to an increase or decrease in the buoyancy force compared to uniform heat flux distribution, as shown in Table 4.4. The highest increase and decrease in mass flow rate are for Gaussian and non-linear increasing heat flux distribution, respectively as compared to uniform heat flux distribution.

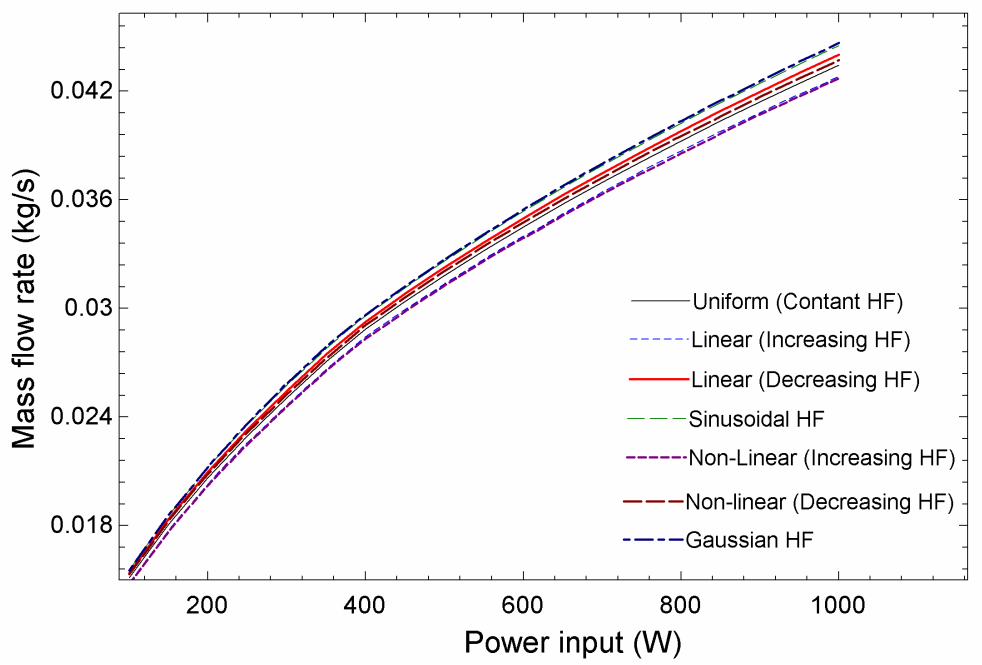

Fig. 4.14 Effect of different heat flux distribution nature on steady mass flow rate for Al_2O_3+Cu +Water.

Table 4.4 Buoyancy force calculation for different nature of heat flux distribution.

Nature of heat flux	Buoyancy force (N/m^3)	Change in buoyancy force as compared to that of uniform heat flux (%)
Uniform	851	_

Linear increasing	827	2.9 (decrement)
Linear decreasing	875	2.72 (Increment)
Sinusoidal	890	4.58 (Increment)
Non-linear increasing	820	3.64 (decrement)
Non-linear decreasing	868	2.72 (Increment)
Gaussian	892	4.82(Increment)

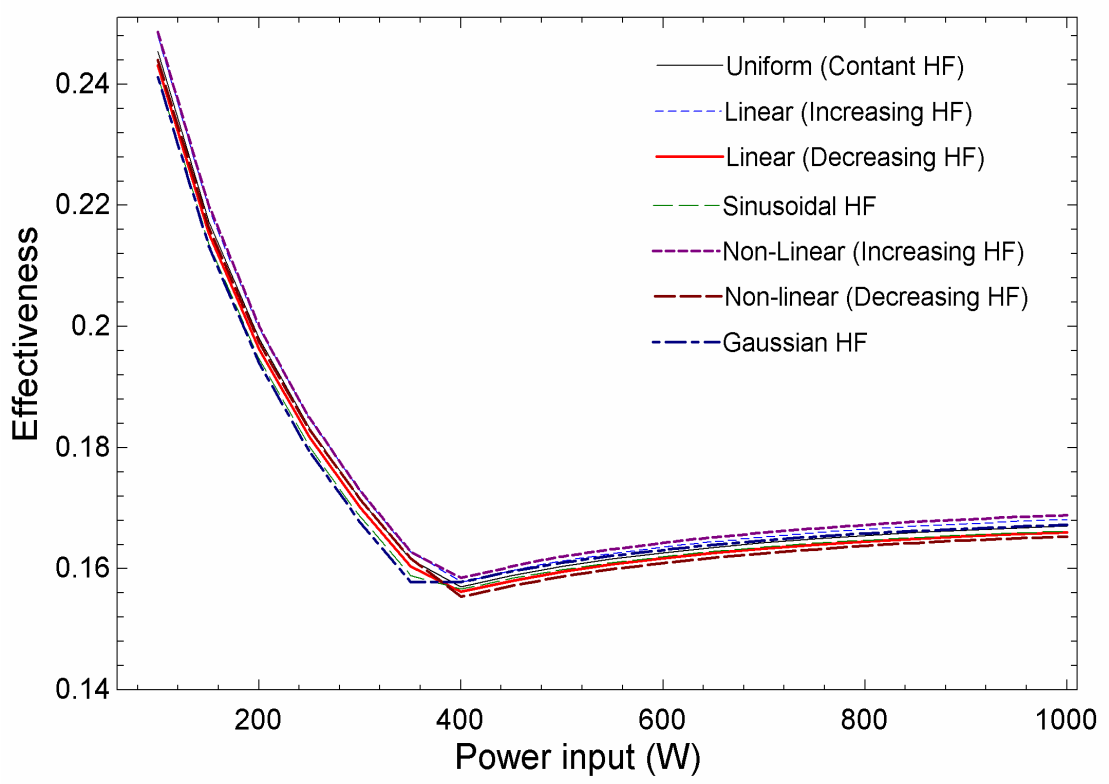

Fig. 4.15 Effect of different heat flux distribution nature on effectiveness for Al_2O_3+Cu +Water.

Fig.4.15 shows the effect of the different nature of heat flux distribution on cooler effectiveness with power input for Al_2O_3+Cu +Water. Figures 4.15 illustrates the effectiveness decreases and then increases with the power input. This is due to switching of Nusselt correlation at Re=2500 at approximately 400 W. The effectiveness decreases and then increases with the power input. The reason may be that increasing power input

both the numerator and denominator term in the effectiveness equation (4.26) increases. The increment in the numerator is lower compared to the denominator up to Re=2500 due to the lower heat transfer coefficient and higher after Re=2500 due to a higher heat transfer coefficient. The effectiveness is highest for Non-linear increasing heat flux for both laminar and turbulent flow regimes, whereas the lowest for Gaussian heat flux in laminar and Non-linear decreasing heat flux distribution in the turbulent flow regimes. The effectiveness is higher due to the higher temperature difference between the hot and cold leg can be seen in the Fig.4.15. at 500 power input. Fig.4.16 shows the temperature distribution along the loop length for different heat flux distribution at 500 W, which falls in the turbulent flow regime. Figure 4.16 also reveals that the Non-linear decreasing heat flux shows the lowest maximum temperature in the loop for the same power input, which means this nature of heat flux can be operated for higher power input for SPNCL by avoiding phase change.

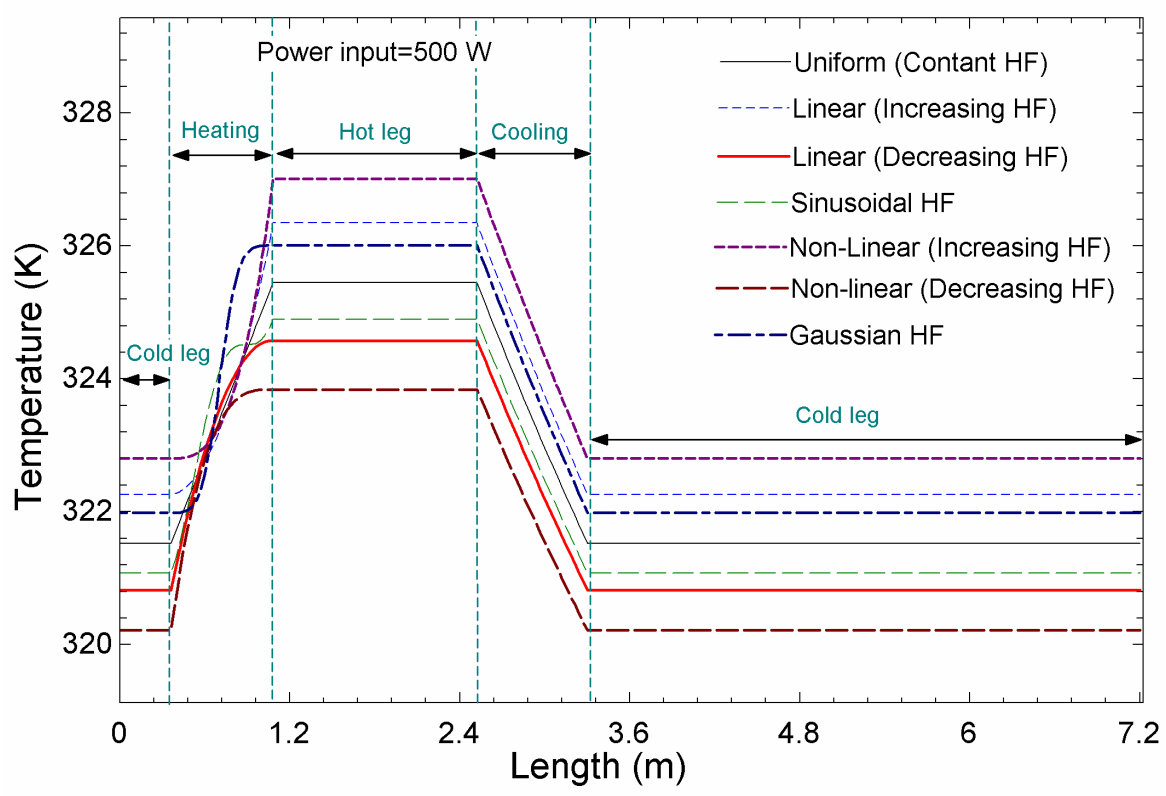

Fig. 4.16Temperature distribution along loop length for different heat flux distribution nature for Al_2O_3+Cu +Water.

Fig.4.17 shows the influence of power input on the total entropy generation rate for different nature heat flux distribution. Figure 4.17 portrays that the total entropy generation increases with the power input. This is because the cause of entropy generation is the irreversibility connected with the heat transfer and pressure drop. Both heat transfer rate and pressure drop (due to increased mass flow rate) increase with power input and the irreversibility associated with it also increases. Hence the total entropy generation rate increases. The total entropy generation rate is highest for Non-linear increasing heat flux and lowest for non-linear decreasing heat flux distribution. Lower total entropy generation shows the good energetic performance of the SPNCL system.

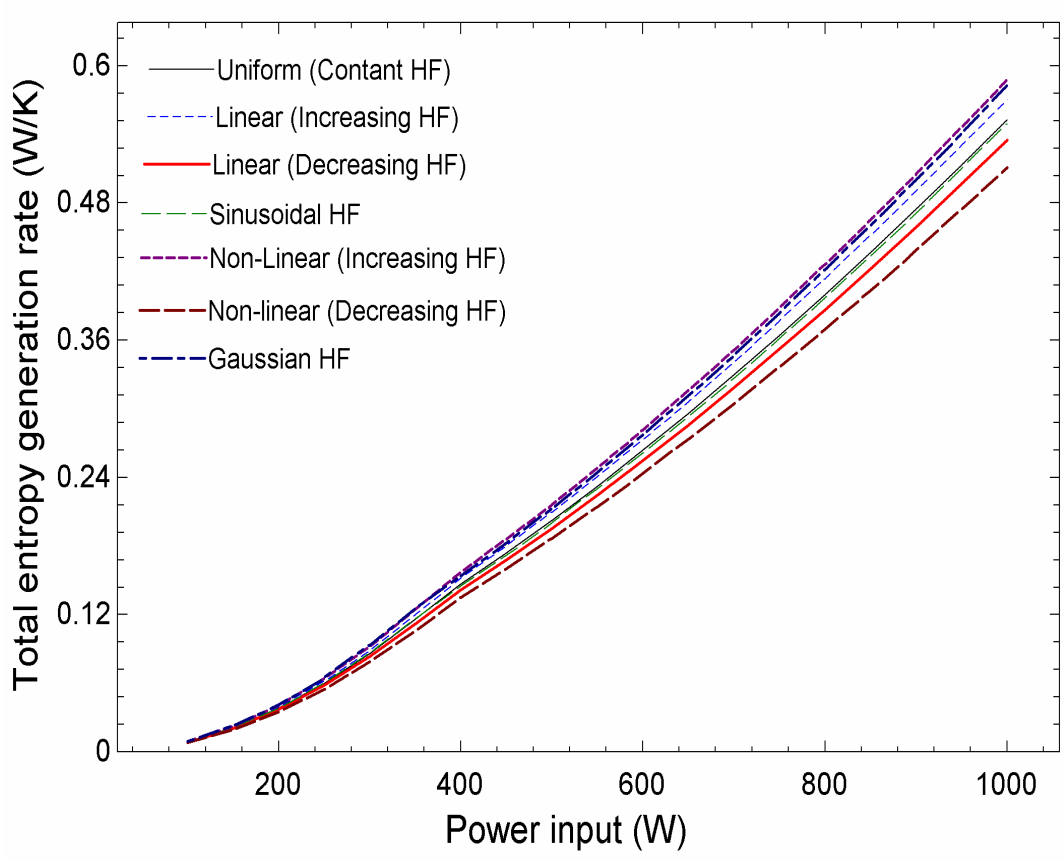

Fig. 4.17 Effect of different heat flux distribution nature on total entropy generation for Al_2O_3+Cu +Water.

4.3 Important highlights

The present analysis explored the transient and steady-state characteristics of a rectangular VHHC single-phase NCL using different cases of assumption, working fluids and nature of heat flux distribution on the performance parameters. Some major findings are summarized as follows:

- Non-Boussinesq (with temperature-dependent other properties, conduction effect, bend effect and heat loss) predicts the close agreement with the experimental result for both steady and transient behavior of SPNCL.
- Boussinesq approximation with constant other properties underpredict and Non-Boussinesq with variable other properties overpredicts the steady mass flow rate. Whereas both underpredicts the effectiveness and overpredict the total entropy generation.
- The conduction effect increases the mass flow rate, and total entropy generation rate and decreases the effectiveness of the cooler. Whereas heat loss and bend effect reduces the mass flow rate and increases the effectiveness. Moreover, the entropy generation rate increases for bend effect and decreases for heat loss.
- Using Boussinesq approximation with constant other properties, the error in the performance parameter is higher for EG and PG brine fluids, which restricts the implication of Boussinesq approximation for all the fluids.
- Boussinesq approximation with constant other properties underpredicts the fluid flow initiation as compared to the actual case represented by Non-Boussinesq with temperature-dependent other properties (with conduction effect, bend effect and heat loss).
- The Gaussian heat flux distribution shows the highest and non-linear increasing heat flux shows the lowest mass flow rate at a given power input. Whereas non-linear

increasing heat flux shows the highest and non-linear decreasing heat shows the lowest effectiveness and total entropy generation rate.

- The fluctuation in the mass flow rate and the time required to attain a steady-state is highest for non-linear decreasing heat flux
- The wall conduction is an important parameter because it imparts a time delay for the initiation of transient flow conditions. The bend introduces additional substantial flow resistance, which leads to the reduction of amplitude of mass flow rate.
- Non-Boussinesq approximation, along with the temperature-dependent variation of other properties, is recommended for reproducing the correct behavior of SPNCL.